PROCEEDINGS, 47th Workshop on Geothermal Reservoir Engineering
Stanford University, Stanford, California, February 7-9, 2022
SGP-TR-223

Developing a comprehensive seismic catalog using a matched-filter detector during a 2019 stimulation at Utah FORGE

Alex Dzubay[1], Maria Mesimeri[2], Katherine M. Whidden[1], Daniel Wells[1], Kris Pankow[1]

[1] University of Utah Seismograph Stations, University of Utah, Salt Lake City, UT, USA

[2] Swiss Seismological Service, ETH-Zurich, Zurich, Switzerland

u1130950@utah.edu

Keywords: FORGE, microseismicity, correlation, b-value, Utah

ABSTRACT

In April 2019, a stimulation was carried out at the Utah Frontier Observatory for Research in Geothermal Energy (FORGE). Microseismicity during this stimulation was monitored using 1) a geophone string and DAS cable in a collocated borehole, 2) a local network of surface broadband sensors and a 305 m shallow borehole geophone, and 3) a surface network of geophones. The detection capabilities of this network were mixed. The most complete catalog, which contains 424 events spanning -2.0 M_w to -0.5 M_w, was determined using the geophone string operated by Schlumberger. However, this catalog is limited by short monitoring duration, which restricts seismic observations to the injection times. Here, we implement a matched-filter detector using a single borehole station within the FORGE footprint to identify small earthquakes ($M_w < 0$) which previously went undetected. Matched-filter detectors are widely used to develop comprehensive earthquake catalogs that can provide better estimations of the Gutenberg-Richter *b*-value, which is a valuable tool in the development of site-specific seismic mitigation strategies and protocols such as Adaptive Traffic Light Systems (ATLS). The goal of this analysis is to use these detections to 1) determine the detection capabilities for the sensors in the shallow borehole, 2) determine the duration of seismic activity associated with the 2019 stimulation, and 3) enhance the catalog to produce a robust *b*-value estimation. These data provide a workflow for future studies focused on characterizing the seismic hazard near potential Enhanced Geothermal Systems, especially those which are in relatively aseismic areas.

1. INTRODUCTION

Enhanced Geothermal Systems (EGS) have the potential to provide reliable, low-cost, energy in a safe and sustainable manner. Unfortunately, previous oversights in the implementation and research of EGS have resulted in a lack of confidence and support from the public and commercial investors. In 2018, the U.S. Department of Energy's Frontier Observatory for Research in Geothermal Energy (FORGE) project was established with the goal of generating groundbreaking research on EGS while demonstrating to the public and private sectors that EGS can be developed and maintained safely. Since its inception, FORGE has published numerous studies related to site characterization, seismic monitoring, and drilling technology (e.g. Moore et al., 2021; Sugiura et al., 2021; Finnilia, 2021; Xing et al., 2021; Nadimi et al., 2020; Xing et al., 2022). In spring of 2019, a stimulation was carried out in well 58-32, a 2290 m deep vertical borehole at the FORGE site near Milford, Utah. Figure 1 shows the layout of the FORGE footprint, including the nearby Mag Lee and Opal Mound Faults which bound the Roosevelt Hot Springs geothermal area to the east. The purpose of the stimulation, which was performed in three stages, was to produce additional characterization of the reservoir rocks at FORGE. In the first stage, the open hole section at the bottom of the well was stimulated over April 21 – April 24 to determine stress orientations and magnitudes as well as permeability. For the second and third stages, which were conducted over April 26 – April 28 and April 30 – May 2, two perforated sections near the bottom of the well casing were stimulated to test the viability of stimulating fractures with different orientations behind casing. Seismic monitoring of this stimulation was performed using various methods including a surface nodal array, a local network of surface broadband sensors and 305 m shallow borehole geophones, as well as DAS. The most complete of these monitoring techniques was a 12-level string of geophones deployed in well 78-32 and operated by Schlumberger. The catalog compiled by Schlumberger contains over 420 microseismic events.

One of the largest obstacles to the widespread implementation of EGS is induced seismicity, which has forced previous EGS research projects to end prematurely (Kraft & Deichmann, 2014; Ellsworth et al., 2019). However, other studies have shown that site-specific seismic mitigation strategies and protocols such as Adaptive Traffic Light Systems (ATLS) can be safely executed (Kwiatek et al., 2019). A key aspect of many seismic mitigation strategies is an estimation of the *b*-value, which represents the slope of the frequency-magnitude distribution of earthquakes in log-linear space as defined by the Gutenberg-Richter (G-R) law (Gutenberg and Richer, 1944). The utility of the *b*-value stems from its ability to characterize the relative likelihood of small versus large earthquakes in a certain region, but the *b*-value also communicates information regarding the state of stress on faults in the area (Amitrano, 2003; Scholz, 2015; Schorlemmer et al., 2005). Previous studies focused on seismic mitigation strategies have used the *b*-value to perform various methods of induced seismicity forecasting including time-varying seismic hazard assessment (Bachmann, 2011; Mena et al., 2013) and maximum magnitude estimation (Shapiro et al., 2011; van der Elst et al., 2016). Critical to the process of *b*-value estimation is an accurate calculation of the magnitude of completeness (M_c), which is defined as the lowest magnitude at which all earthquakes in a space-time window are detected (Rydelek & Sacks, 1989). Incorrect assessments of M_c have a direct impact on the calculation of *b*-value, leading to inaccurate seismic hazard evaluations and earthquake forecast models (Woessner & Wiemer, 2005). Additionally,

earthquake catalogs that do not contain enough events to characterize the G-R distribution over a considerable magnitude range will also generate unreliable G-R parameter estimations (Knopoff et al., 1982, Kagan, 2004).

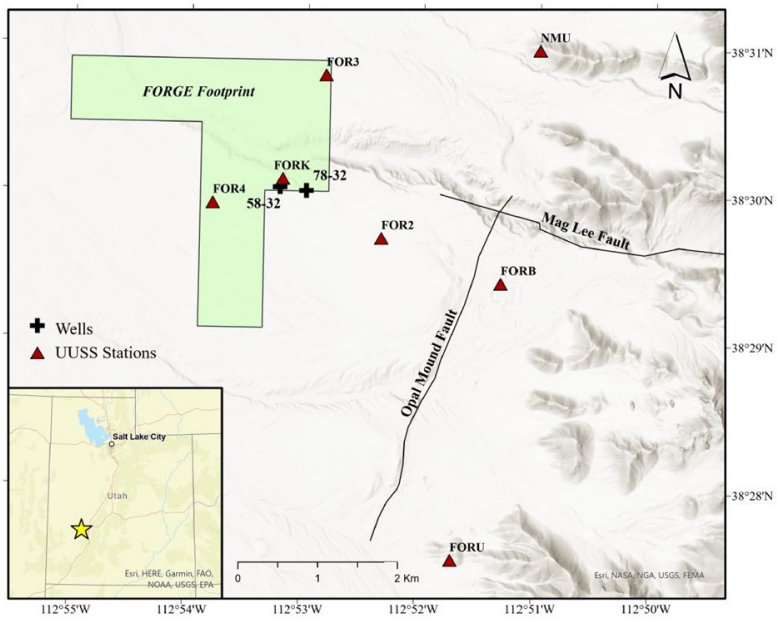

Figure 1: Layout of the FORGE site and surrounding area. Red triangles represent permanent seismic stations operated by University of Utah Seismograph Stations. Black crosses show the location of wells used in the 2019 stimulation. Star shows the location of FORGE within the state of Utah.

In this study, we aim to 1) determine the detection capabilities for the FORK seismic sensors 2) determine the duration of seismic activity associated with the 2019 stimulation, and 3) provide a robust estimate for the *b*-value at Utah FORGE. To address these issues, we implement a matched-filter detector using continuous data from seismic station FORK located within the FORGE footprint to detect small ($M_w < 0$), previously undetected earthquakes. Matched-filter detectors are widely used to develop comprehensive earthquake catalogs and improve the detection capabilities of local networks (e.g. Mesimeri et al., 2021a; Schaff & Waldhauser, 2010; Herrmann et al., 2019; Plenkers et al., 2013; Shelley et al., 2016). In this case, the matched-filter detector greatly improves the detection capabilities of the FORK station, which suffered from a very low signal-to-noise ratio during the stimulation as a result of its relatively shallow depth and proximity to well 58-32. An enhanced catalog is necessary because the Schlumberger earthquake catalog is restricted to times of active pumping, making an accurate assessment of M_c impossible. Moreover, the use of a matched-filter detector allows for the detection of events occurring between and after the stimulations, providing a more holistic view of seismicity in this timeframe. As a result, we generate a larger, more comprehensive seismic catalog for which a justifiable M_c can be determined. Using this expanded catalog, we estimate the *b*-value at Utah FORGE using both traditional methods (Aki, 1965) and a new method, *b*-positive (van der Elst, 2021), an intriguing technique that is well suited for small, heterogeneous earthquake catalogs.

2. DATA & PREPROCESSING

Within this study are two separate datasets which are used to construct a single earthquake catalog for *b*-value estimation. The first is the seismic catalog compiled by Schlumberger using a string of 12 geophones deployed in well 78-32 between 645 and 981 m (Fig. 1). Using this geophone string, Schlumberger detected and located over 420 events spanning -2.0 M_w to -0.5 M_w during the 2019 stimulation. Unfortunately, this geophone string was only active during the three stimulations, so the Schlumberger catalog is insufficient when attempting to analyze seismicity in this region in and around the time of the stimulations. To address this temporal incompleteness, six weeks of data from the composite borehole station FORK, which was continually running beyond April 23rd, is also used. Because this study requires the detection of microseismic events, we use data from the three-component, short-period sensor at FORK, which has a sample rate of 1000 Hz. In the interest of computational efficiency, we first downsample 24-hr segments of the data to 500 Hz. Next, we detrend the data and apply a Hann window taper. Spectral analysis of the continuous data and Schlumberger events revealed electrical noise at high frequencies and a dominant frequency range of 20-50 Hz for microseismicity; therefore, we apply a 15-60 Hz Butterworth bandpass filter to the 24-hr streams.

3. METHODS

3.1 Matched-filter detector

We apply a matched-filter method following the process of Mesimeri et al. (2021a) to detect new earthquakes at the FORK station. First, twelve events from the Schlumberger catalog were selected as templates due to their relatively high signal-to-noise ratio. We use 90 s long waveforms from the FORK dataset starting at the origin time for each of these template events and carry out data preprocessing identical to that of the 24-hr streams. Next, P-phase templates are obtained from the vertical channel using a 0.4 s window

starting 0.1 s before the manually picked P arrival and ending 0.3 s after the P arrival. S-phase templates are extracted from the horizontal channels using a 0.5 s window starting 0.1 s before the manual S pick and ending 0.4 s after the S arrival. Note that these relatively short windows are appropriate because of the small magnitude and short duration of the template events. After preparing the templates, we then apply the matched-filter to each channel of a 24-hr stream with a corresponding template, calculating a Pearson correlation coefficient time series which is shifted by that template's arrival time. Finally, the cross-correlation time series for all phases and channels are summed to create stacked correlation coefficient time series for each day and template event.

Detections are recorded when the correlation coefficient exceeds 8 times the median absolute deviation (8*MAD); however, we apply three additional steps of quality control to manually verify each detection (Fig. 2). First, a visual inspection of the detection waveform with the corresponding templated overlayed is performed to ensure the matched-filter detector was not triggering on electrical or pumping noise. Next, a spectrogram of the waveform is analyzed to determine if the detection exhibits frequency content in the expected range of 20-50 Hz for microseismicity in the region. Finally, we perform frequency domain detection analysis as in Mesimeri et al. (2021b), taking advantage of the high S wave energy in these events to effectively quantify the previous step. To carry out this analysis, we first perform spectral whitening using a normalization window that is 20 times the duration of the seismic signal. Following normalization, we obtain a trace describing signal power by summing the amplitudes over a 20-50 Hz frequency band. One final summed power trace is obtained for each detection by stacking the traces from each component after removing the mean and computing the envelopes for the summed amplitudes. Peaks of the summed trace therefore highlight seismic signals with distinctive frequency content. Though this method of quality control was time consuming, the small scope of this study made it feasible to use this process to ensure no false detections were included in the final catalog. Future studies will automate the quality control process by optimizing the method of frequency domain detection analysis.

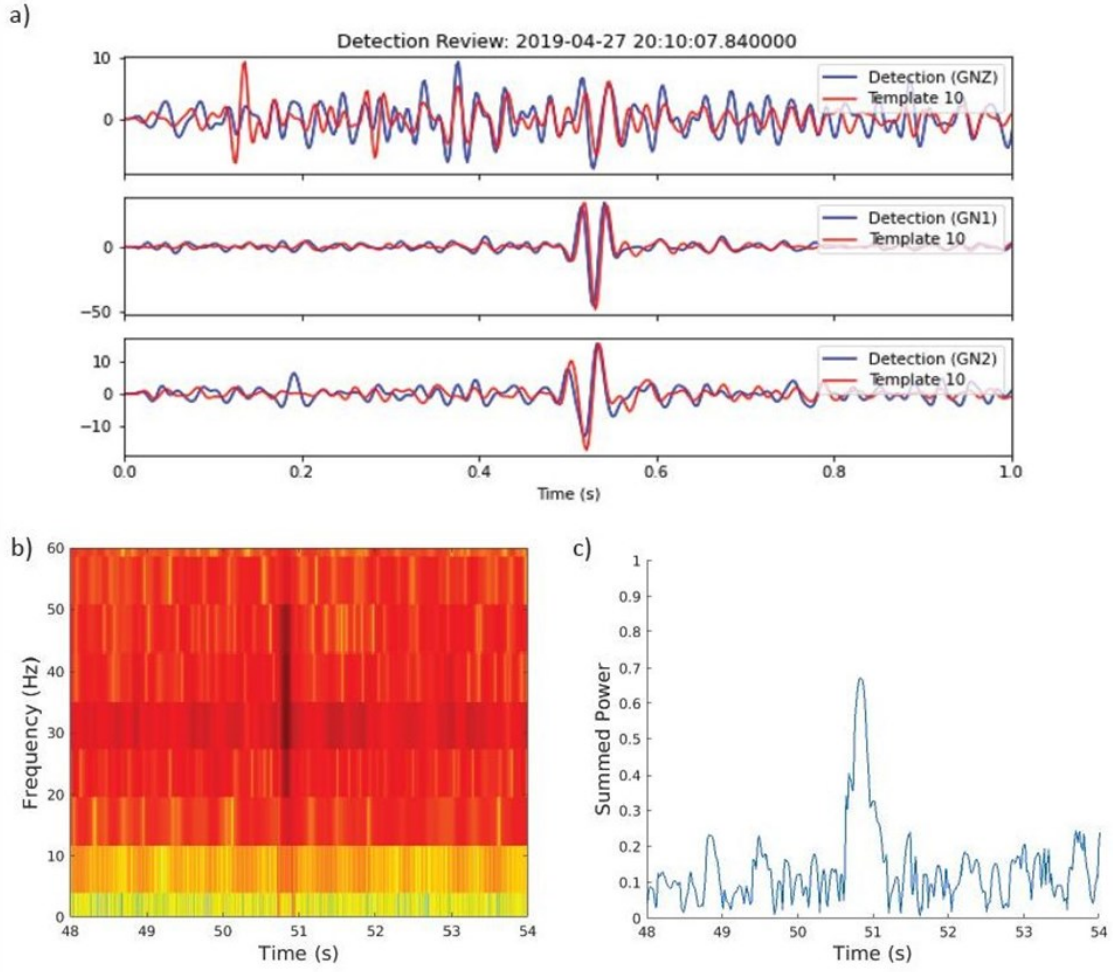

Figure 2: Summary of matched-filter method and quality control process. (a) Visual comparison of detected waveform (blue) overlayed with the template used to make the detection (red) for all three components. (b) Spectrogram of the detected waveform. (c) Trace generated for frequency domain detection analysis by summing normalized amplitudes over a 20-50 Hz frequency band.

After running all twelve original templates across the specified timeframe, we then select 17 detections with the highest signal-to noise ratios to be used as a second round of template events. Following the completion of this second round, one additional step was required

to ensure the detected events accurately describe the seismicity in the FORGE area. Specifically, all detected events with S-P times greater than 0.5 s were removed after it was determined that some of these events may have originated in the Roosevelt Hot Springs geothermal area. Magnitudes for approved detections are generated using the median of the maximum amplitude ratios between the detection and template event. These magnitudes are relative, assuming a tenfold increase in amplitude corresponds to one unit increase in magnitude (Peng & Zhao, 2009). To test the accuracy of the relative magnitudes of these detections, we plot the matched-filter magnitudes against Schlumberger-calculated magnitudes for events that are found in both catalogs (Fig. 3). This test illuminates a small discrepancy towards the underestimation of matched-filter magnitudes, so we apply a 0.2 M_w shift to all matched-filter events.

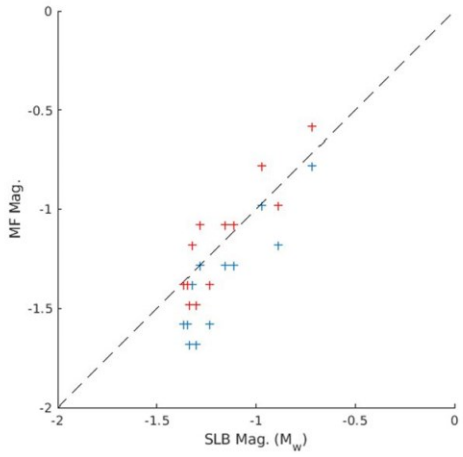

Figure 3: Comparison between relative magnitudes determined using amplitude ratios (MF) and moment magnitudes calculated by Schlumberger (SLB). Blue crosses show the original magnitudes, red crosses show the shifted magnitudes, and the black dashed line represents a 1:1 relation.

3.2 B-value estimation

In the interest of obtaining a robust estimate for the *b*-value in the FORGE area during the stimulation, we perform the calculation with two different approaches. In addition, we obtain *b*-value estimates for all three catalogs (matched-filter, Schlumberger, and combined) to gain insight into the influences affecting the final b-value estimations. For the first method, we determine Mc using the maximum curvature method and a +0.2 correction (Wiemer and Wyss, 2000). *B*-values are then calculated using the traditional method of maximum likelihood (Aki, 1965) and we estimate error following the process of Shi and Bolt (1982).

For the second approach, we apply a new method called *b*-positive (van der Elst, 2021). This recently developed estimator relies on the fact that a subset of all positive differences in magnitude between successive earthquakes within a catalog can be described by a double-exponential distribution with the same scale parameter as the frequency-magnitude distribution. This approach is advantageous because the distribution of magnitude differences is perturbed far less by large earthquakes, making the technique well-suited for relatively small earthquake catalogs. In addition, because these differences are limited to successive earthquakes, the *b*-positive estimator is insensitive to M_c, greatly increasing its robustness in heterogeneous catalogs where M_c may vary considerably. Moreover, because only positive magnitude differences are considered, the estimate is much more resistant to short-term aftershock incompleteness which saturates negative magnitude differences. Catalog incompleteness can still affect the distribution of magnitude differences, so we determine the minimum magnitude difference (dM_c) using the same the maximum curvature method and a +0.2 correction. Encouraged by the potential benefits of this technique, we calculate *b*-positive estimates using the maximum likelihood method on the double-exponential distribution of positive magnitude differences for all three catalogs, estimating error again following Shi and Bolt (1982).

4. RESULTS

Upon completion, the two rounds of matched-filter application generated 613 and 373 detections, respectively. After applying the quality control process, the first round retained 89 approved detections and the second round retained 122. After the final step of removing events with S-P > 0.5 s, the matched-filter catalog consists of 133 unique events. Accounting for both rounds of matched-filter detection and Schlumberger events, the final combined catalog contains a total of 534 microseismic events spanning -2.0 M_w to -0.1 M_w. Figure 4 illustrates the distribution of these events with respect to time and magnitude. Of the 133 matched-filter events spanning -1.8 M_w to -0.1 M_w in the combined catalog, 111 were not recorded by Schlumberger. These unique matched-filter events provide a more comprehensive view of the seismicity during the stimulation timeframe, confirming that seismicity was persistent both in between and following the three stages of pumping. In terms of detection threshold, the matched-filter detector performs slightly worse than the 12-level string of geophones, recording no earthquakes smaller than -1.8 M_w. This is to be expected, however, as the geophone string was recording at a much greater depth, which limited pumping noise. The number of detections begins to decrease in mid-to-late May, nearly a month after the last stage of the stimulation, though one of the largest earthquakes (-0.2 M_w) was recorded in this timeframe.

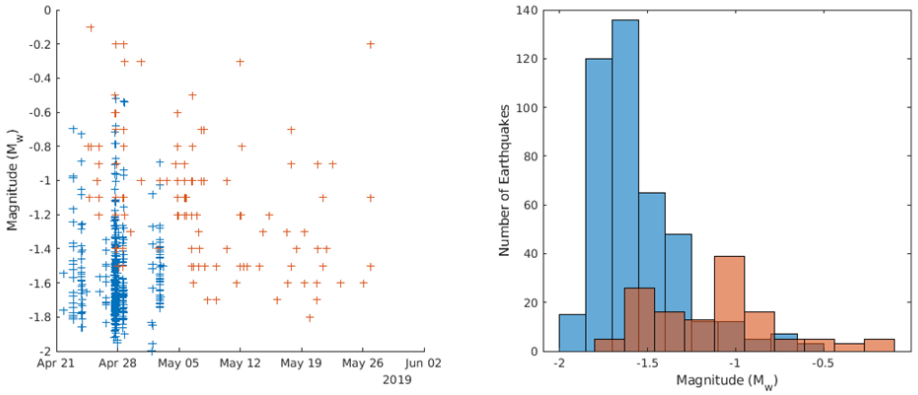

Figure 4: Overview of the resulting seismic catalog following the use of the matched-filter detector. (Left) Magnitude-time distribution of matched-filter events (orange) and Schlumberger events (blue). (Right) Frequency-magnitude distribution for both catalogs using the same color conventions.

Figure 5 presents the results of our M_c and dM_c calculations for each of the three catalogs: matched-filter, Schlumberger, and combined. Evidently, the matched-filter catalog produces the most unstable frequency-magnitude distribution, and a relatively high value of M_c (Fig. 5a). The disparity between the M_c of the Schlumberger catalog (-1.5 M_w, Fig. 5b) and the matched-filter catalog (-0.9 M_w, Fig. 5a) is larger than expected if considering their different detection thresholds, emphasizing the sparsity of the matched-filter catalog. Note that the calculations of M_c and dM_c for the Schlumberger catalog are technically inaccurate because there are missing events between stimulation stages. Therefore, the combined catalog (Fig. 5c) must be assigned the same M_c as the matched-filter catalog to account for time periods when the geophone string was inactive. The three magnitude difference distributions appear to be more stable and produce similar values for dM_c. In this case, the combined catalog is not assigned the dM_c of the matched-filter catalog because a higher value was calculated naturally.

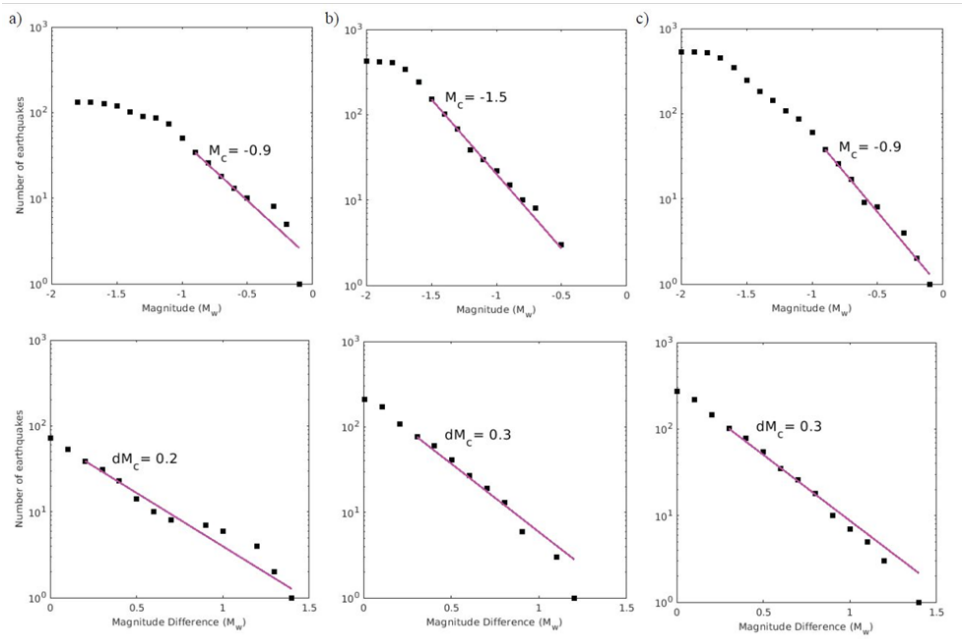

Figure 5: Results of the maximum curvature tests used to determine M_c (Top) and dM_c (Bottom) for the (a) matched-filter, (b) Schlumberger, and (c) combined seismic catalog. Black squares show the cumulative distribution of earthquakes in a certain magnitude or magnitude difference bin. Purple lines show the trend described by *b*-value estimates.

Results from the two different methods for estimating *b*-value are displayed in Figure 6. Additionally, Table 1 lists the final *b*-value estimates from each method for all catalogs. These values represent tentative estimates determined from fewer than 500 events, and the *b*-values are therefore reported in the form of 95% confidence intervals. The performances of both methods vary among the catalogs, but the *b*-positive estimates are undoubtably more stable, generating smaller errors than the traditional G-R method for all three catalogs. The estimate that we consider the most robust comes from applying the *b*-positive method to the combined catalog and results in a value of 1.61 ± 0.16.

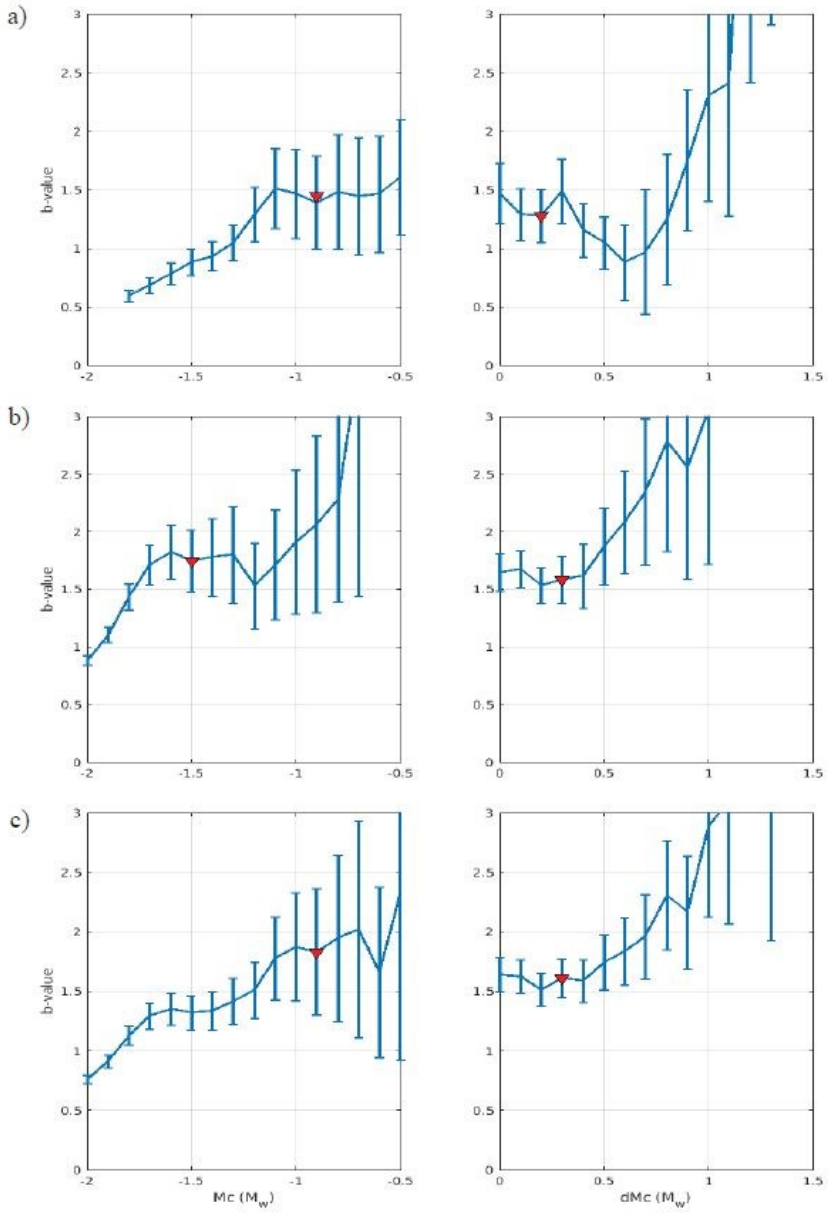

Figure 6: Results of *b*-value estimation for the (a) matched-filter catalog, (b) Schlumberger catalog, and (c) combined catalog. (Left) Traditional method of maximum likelihood applied using the G-R Law. (Right) *B*-positive technique of applying maximum likelihood to distribution of positive, successive magnitude differences. Error bars represent the 95% confidence interval. Red triangles show the associated M_c and dM_c found in Fig. 5.

Table 1: Summary of *b*-value estimates.

	Traditional G-R			*B*-positive (b^+)		
Catalog	M_c (M_w)	b	95% Confidence	dM_c (M_w)	b^+	95% Confidence
Matched-filter	-0.9	1.39	$1.00 \leq b \leq 1.79$	0.2	1.28	$1.05 \leq b^+ \leq 1.51$
Schlumberger	-1.5	1.75	$1.48 \leq b \leq 2.02$	0.3	1.59	$1.38 \leq b^+ \leq 1.79$
Combined	-0.9	1.83	$1.30 \leq b \leq 2.37$	0.3	1.61	$1.45 \leq b^+ \leq 1.77$

4. CONCLUSION

We present a study in which a matched-filter detector is used to expand the earthquake catalog associated with a stimulation performed at the Utah FORGE site in spring of 2019. Events found using the matched-filter detector expand our understanding of the seismicity associated with the stimulation, confirming that earthquakes continued to occur both in between and up to a month after the three stages of injection with one of the larger events, -0.2 M_w, occurring 24 days after pumping stopped. Moreover, the catalog generated from the detector shows that future studies using a matched-filter detector on the FORK borehole station will encounter a detection threshold near -1.8 M_w. Both traditional G-R techniques and a new method called *b*-positive are used to estimate the *b*-value at the Utah FORGE site. Out of the two techniques, *b*-positive produced estimates that were considerably more stable than those calculated using the traditional G-R approach. This improvement is likely a result of the *b*-positive estimator's resilience to large earthquake perturbations and M_c variation. We report a final *b*-value estimate of 1.61 ± 0.16 with 95% confidence for the combined catalog. These data provide a new, more dependable estimate for modeling purposes at Utah FORGE. More importantly, this study provides further evidence of the capabilities of *b*-positive while acting as a basis for future studies focused on characterizing the seismic hazard at EGS sites in relatively aseismic areas. Future research at Utah FORGE will optimize this workflow for larger applications during future stimulations.

ACKNOWLEDGEMENTS

We thankfully acknowledge the support given by Nicholas van der Elst in applying the *b*-positive technique to this dataset. Furthermore, we thank Schlumberger for compiling the initial earthquake catalog used in this study. Funding was provided by DOE EERE Geothermal Technologies Office under Project 429 DE-EE0007080 Enhanced Geothermal System Concept Testing and Development at the Milford City, Utah Frontier Observatory for Research in Geothermal Energy (FORGE) site and the State of Utah. The support and resources from the Center for High Performance Computing at the University of Utah are gratefully acknowledged. Waveforms from FORGE stations are available through the University of Utah Seismograph Stations (https://quake.utah.edu/FORGE-map) and through Incorporated Research Institutions for Seismology (www.iris.edu/hq/; network code UU).

REFERENCES

Aki, K.. Maximum likelihood estimate of b in the formula log N=a-bM and its confidence limits. Bull. Earthq. Res. Inst., Univ. Tokyo, 43, (1965), 237–239.

Amitrano, D.. Brittle-ductile transition and associated seismicity: Experimental and numerical studies and relationship with the b value. Journal of Geophysical Research: Solid Earth, 108(B1), (2003).

Bachmann, C. E.. New approaches towards understanding and forecasting induced seismicity (Doctoral dissertation, ETH Zurich), (2011).

Ellsworth, W. L., Giardini, D., Townend, J., Ge, S., and Shimamoto, T.. Triggering of the Pohang, Korea, Earthquake (Mw 5.5) by Enhanced Geothermal System Stimulation. Seismological Research Letters, 90(5), (2019), 1844–1858.

Gutenberg, B., and Richter, C. F.. Frequency of earthquakes in California*. Bulletin of the Seismological Society of America, 34(4), (1944), 185–188.

Herrmann, M., Kraft, T., Tormann, T., Scarabello, L., and Wiemer, S.. A Consistent High-Resolution Catalog of Induced Seismicity in Basel Based on Matched Filter Detection and Tailored Post-Processing. Journal of Geophysical Research: Solid Earth, 124(8), (2019), 8449–8477.

Kagan, Y. Y.. Short-Term Properties of Earthquake Catalogs and Models of Earthquake Source. Bulletin of the Seismological Society of America, 94(4), (2004) 1207–1228.

Knopoff, L., Kagan, Y. Y., and Knopoff, R.. Values for foreshocks and aftershocks in real and simulated earthquake sequences. Bulletin of the Seismological Society of America, 72(5), (1982) 1663–1676.

Kraft, T., & Deichmann, N.. High-precision relocation and focal mechanism of the injection-induced seismicity at the Basel EGS. Geothermics, 52, (2014) 59–73.

Kwiatek, G., Saarno, T., Ader, T., Bluemle, F., Bohnhoff, M., Chendorain, M., Dresen, G., Heikkinen, P., Kukkonen, I., Leary, P., Leonhardt, M., Malin, P., Martínez-Garzón, P., Passmore, K., Passmore, P., Valenzuela, S., and Wollin, C. (2019). Controlling fluid-induced seismicity during a 6.1-km-deep geothermal stimulation in Finland. Science Advances, 5(5), (2019).

Mena, B., Wiemer, S., and Bachmann, C.. Building Robust Models to Forecast the Induced Seismicity Related to Geothermal Reservoir Enhancement. Bulletin of the Seismological Society of America, 103(1), (2013) 383–393.

Mesimeri, M., Pankow, K. L., Baker, B., and Hale, J. M.. Episodic Earthquake Swarms in the Mineral Mountains, Utah Driven by the Roosevelt Hydrothermal System. Journal of Geophysical Research: Solid Earth, 126(6), (2021a).

Mesimeri, M., Pankow, K. L., and Rutledge, J.. A Frequency-Domain-Based Algorithm for Detecting Microseismicity Using Dense Surface Seismic Arrays. Bulletin of the Seismological Society of America, 111(5), (2021b), 2814–2824.

Moore, J., McLennan, J., Pankow, K., Simmons, S., Podgorney, R., Wannamaker, P., Jones, C., Rickard, W., and Xing, P.. The Utah Frontier Observatory for Research in Geothermal Energy (FORGE): A Laboratory for Characterizing, Creating and Sustaining Enhanced Geothermal Systems. 45th Workshop on Geothermal Reservoir Engineering, Stanford University, Stanford, CA (2020).

Nadimi, S., Forbes, B., Moore, J., Podgorney, R., and McLennan, J. D.. Utah FORGE: Hydrogeothermal modeling of a granitic based discrete fracture network. Geothermics, 87, (2020).

Plenkers, K., Ritter, J. R. R., and Schindler, M.. Low signal-to-noise event detection based on waveform stacking and cross-correlation: application to a stimulation experiment. Journal of Seismology, 17(1), (2013), 27–49.

Rydelek, P. A., and Sacks, I. S.. Testing the completeness of earthquake catalogues and the hypothesis of self-similarity. Nature, 337(6204), (1989), 251–253.

Schaff, D. P., and Waldhauser, F.. One Magnitude Unit Reduction in Detection Threshold by Cross Correlation Applied to Parkfield (California) and China Seismicity. Bulletin of the Seismological Society of America, 100(6), (2010), 3224–3238.

Scholz, C. H.. On the stress dependence of the earthquake b value. Geophysical Research Letters, 42(5), (2015), 1399–1402.

Schorlemmer, D., Wiemer, S., and Wyss, M.. Variations in earthquake-size distribution across different stress regimes. Nature, 437(7058), (2005), 539–542.

Shapiro, S. A., Krüger, O. S., Dinske, C., and Langenbruch, C.. Magnitudes of induced earthquakes and geometric scales of fluid-stimulated rock volumes. Geophysics, 76(6), (2011), 55–63.

Shelly, D. R., Ellsworth, W. L., and Hill, D. P.. Fluid-faulting evolution in high definition: Connecting fault structure and frequency-magnitude variations during the 2014 Long Valley Caldera, California, earthquake swarm. Journal of Geophysical Research: Solid Earth, 121(3), (2016), 1776–1795.

Shi, Y., and Bolt, B. A.. The standard error of the magnitude-frequency b value. Bulletin of the Seismological Society of America, 72(5), (1982), 1677–1687.

Sugiura, J., Lopez, R., Borjas, F., Jones, S., McLennan, J., Winkler, D., Stevenson, M., and Self, J.. Oil and Gas Drilling Optimization Technologies Applied Successfully to Unconventional Geothermal Well Drilling. SPE Annual Technical Conference and Exhibition, Dubai, UAE (2021).

van der Elst, N. J.. B-positive: A Robust Estimator of Aftershock Magnitude Distribution in Transiently Incomplete Catalogs. Journal of Geophysical Research: Solid Earth, 126(2), (2021).

van der Elst, N. J., Page, M. T., Weiser, D. A., Goebel, T. H. W., and Hosseini, S. M.. Induced earthquake magnitudes are as large as (statistically) expected. Journal of Geophysical Research: Solid Earth, 121(6), (2016), 4575–4590.

Wiemer, S., and Wyss, M.. Minimum Magnitude of Completeness in Earthquake Catalogs: Examples from Alaska, the Western United States, and Japan. Bulletin of the Seismological Society of America, 90(4), (2000), 859–869.

Woessner, J., and Wiemer, S.. Assessing the Quality of Earthquake Catalogues: Estimating the Magnitude of Completeness and Its Uncertainty. Bulletin of the Seismological Society of America, 95(2), (2005), 684–698.

Xing, P., Damjanac, B., Moore, J., and McLennan, J.. Flowback Test Analyses at the Utah Frontier Observatory for Research in Geothermal Energy (FORGE) Site. Rock Mechanics and Rock Engineering, (2021).

Xing, P., McLennan, J., & Moore, J.. Minimum in-situ stress measurement using temperature signatures. Geothermics, 98, (2022).